Designing photochromic pigments based on clay minerals and spiropyran

Graycyellê R. S. Cavalcanti, Christelle Souprayen, David Guillermin, Francisco Rodrigues, Maria G Fonseca, Maguy Jaber

Designing photochromic pigments based on clay minerals and spiropyran

Graycyellê R. S. Cavalcanti[1,2], Christelle Souprayen[1], David Guillermin[1], Francisco Rodrigues[1,3], Maria G. Fonseca[2,*] and Maguy Jaber[1,4*]

[1]*Sorbonne Université, LAMS, CNRS UMR8220, 75005 Paris, France*

[2]*LACOM, Paraíba Federal University – UFPB, João Pessoa, Paraíba, 58033-455, Brazil*

[3]*LabSAMA, Paraíba State University - UEPB, Campina Grande, Paraíba, 58109-790, Brazil*

[4]*Institut Universitaire de France, Paris, France*

Highlights

- Photochromic hybrid pigments were prepared through adsorption of spiropyran on clay minerals.
- Al-pillared saponite presented high dye adsorption compared to the raw saponite.
- Pigments' colors are pH dependent.
- Reversibility of the colors is light dependent.

***Corresponding authors**
maguy.jaber@upmc.fr ; mgardennia@quimica.ufpb.br

Graphical Abstract

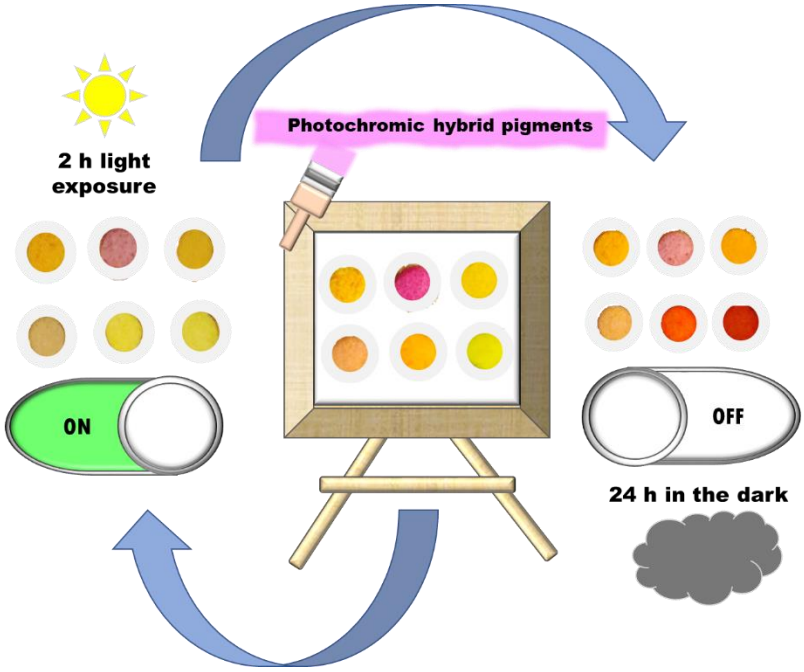

Abstract

Inorganic-organic photochromic hybrid materials have attracted attention in different research fields, since they have a wide potential application in optical memories, sensors, filters, lenses, pigments, and decoration. In this work, the photochromism of the 1-(2-Hydroxyethyl)-3,3-dimethylindolino-6'-nitrobenzopyrylospiran dye was investigated through the preparation of hybrid pigments based on raw and pillared saponites at pH 2 and pH 13 at 25 °C. The second group of pigments was prepared at pH 2 and 25 °C by in-situ hydrolysis of TEOS in the presence of the same dye. All prepared solids were characterized by X-Ray diffraction, ^{13}C CP/MAS NMR and thermogravimetry, and were submitted to irradiation under visible light. The results suggested both intercalation and/or adsorption of the dye onto clay mineral surface via hydrogen bonds for the saponite based pigments. Concerning the hybrids obtained from TEOS hydrolysis reaction, the dye acts as a template resulting in a higher photostability of the resulting pigment compared to those prepared with clay minerals. In general, all hybrid pigments presented photoreversible capacity after light exposure and subsequent time-out in the dark. The findings of this study proposed the multicolored prepared hybrids as promising materials to be applied in photochromic systems as smart pigments.

Keywords: Hybrid pigments, saponite, dyes, photochromic pigments, spiropyran**.**

1. Introduction

Phenomena associated with color variation have been studied in last years in different fields. With regard to pigments, the production of new photochromic materials is highly desired to mimic the occurrence of different types of photochromic transformations observed in nature [1]. Photochromic species present reversible structural transformations over some environmental stimulus including solvents, temperature, presence of metal ions or UV-Vis light irradiation [2,3,4]. The reactivity of the natural systems allows significant changes in the conformation of molecules to occur in response to external stimuli. The latter systems have been inspiring the study and development of new materials with improved properties compared to their isolated form [5,6]. The isomerization caused by light irradiation has advantages associated to the precision and specificity of the molecules, especially if used in light absorption systems [2,3].

Structural and electronic changes in the dye after a specific stimulus allow several photosensitive applications. However, the colorants need to have some properties such as thermal stability of the generated isomers, high sensitivity, rapid response and solid state reactivity, which make their use feasible [7].

Spiropyrans (SPI) are a class of compounds used in the development of multifunctional materials capable of detection [8]. SPI molecules present a reversible photoconversion between two thermodynamically stable states: a form of spiropyran (SP) and a form of merocyanine (MC) where both forms are structurally different and the resulted chemical properties are also distinct (Figure 1) [9,10].

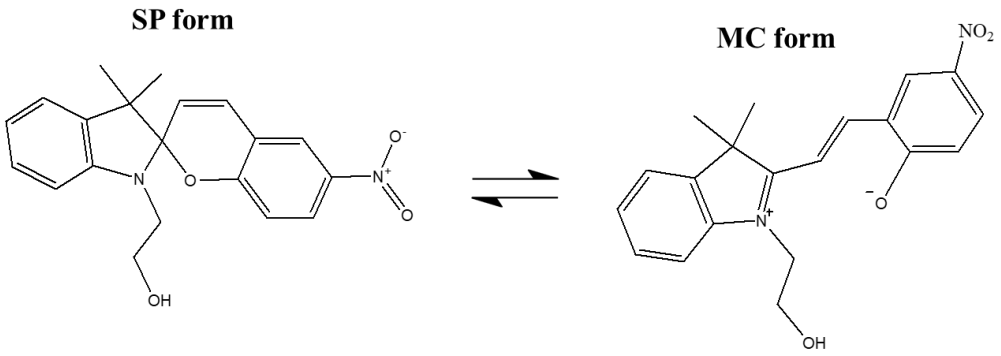

Figure 1- Isomerization between SP and MC forms of the spiropyran structure.

Despite the interesting photochromic properties of the spiropyrans, they have limitations associated to thermal stability under radiation [8]. Moreover, previous studies showed that when spiropyran was attached to a planar surface, it increases the resistance to ‘‘fatigue’’ (gradual degradation with increasing number of switching cycles) in comparison to spiropyran molecules in solution [11].

Development of photosensitive materials based on SPI has been widely reported [7,12,13]. In general, it is desirable to obtain compounds that retain the SPI's molecular interconversion properties and that have additional light and temperature stability properties [8,14]. The preservation of the properties of some SPI after adsorption on aluminium or silicon oxides surfaces and aluminosilicates was documented in the literature. SPI adsorbed on oxide surfaces presented higher reversibility in comparison to the one observed in solution [15]. Two routes are normally used to prepare photochromic hybrid pigments: the encapsulation of the organic dye in inorganic materials through an in-situ approach and the adsorption of the dye on inorganic minerals [16].

Encapsulation can be performed using various techniques such as layer-by-layer assembly and sol-gel method [16–18]. Silica was widely reported for the preparation of hybrid pigments due its transparency and stability. Sol-gel approaches are based on TEOS hydrolysis in an alcohol/water mixtures under acid or basic conditions [19] and the preparation of films

was reported to prevent corrosion, and as a barrier for pigments with aluminum in their composition [20,21].

The methods of preparing pigments by adsorption on inorganic surfaces are inspired by the ancient Maya Blue composed mainly of palygorskite clay and indigo dye. This pigment has demonstrated extraordinary physical-chemical stability and have attracted attention in research worldwide. The development of mimetic new hybrid stable systems containing inorganic surfaces and colorants are highly desired. In this context, layered solids such as double layered hydroxides [22,23], smectites [24,25], palygorskite [26,27] and sepiolites [28,29] have been applied. Saponite is a trioctahedral 2:1 smectite highlighted as an alternative to prepare hybrid pigments thanks to the presence of active sites on its surface and internal exchanged cations in the interlamellar region that allow interaction with chromophores.

In fact, pigments based on raw clay minerals are widely obtained by ion exchange between cationic dyes and interlayer cations of the clay mineral [30]. However, introduction of new functionalities on the clay mineral surface by using organic and/or inorganic modifications are also explored, allowing preparation of new pigments with different chromophores derived from anionic species depending on the desired application [31,32].

Immobilization of SPI on inorganic supports has numerous advantages, such as absence or lower leaching, better mechanical properties, higher solubility, biocompatibility [7,33–35] and reduction in the photodegradation of the dye molecule. The latter aspect is related to a better resistance to photoisomerization and less gradual degradation with cumulative switching cycles [7]. Therefore, the preparation of pigments based on interactions of the dye with inorganic matrices such as silicates or other oxides allows protection of the photosensitive species. Moreover, materials with reversible response present unique possibilities for different applications, such as biosensors, chemical sensors, controlled release, data memory systems, thermal and mechanical sensors, among other applications. [36,37]. Among the numerous

possibilities provided by SPI, the production of pigments allows the creation of new photochromic systems [35]. Dyes such as nitrobenzopyrane and their analogues have been studied to produce pigments, since they have well-established photochemical properties [12,38,39].

In this work, we aimed to synthesize photochromic pigments by using 1-(2-Hydroxyethyl)-3,3-dimethylindolino-6'-nitrobenzopyrylospiran (SPI-H1042; CAS 16111-07-2) immobilized on raw and aluminium pillared saponites. In-situ approach was also used based on TEOS hydrolysis. The resulting pigments were characterized by XRD, thermal analysis and ^{13}C solid state NMR. The photoreversibility under light was tested.

2. Experimental

2.1 Materials

The following chemicals were used as received without prior purification: hydrofluoric acid (40% w/w; Fluka), sodium acetate (99%; Sigma-Aldrich), magnesium acetate (99%; Sigma-Aldrich), aluminium oxide (99.8%; Sigma-Aldrich), silica (Aerosil 380; 99.8%; DEGU), aluminium chloride (99%; Sigma-Aldrich), sodium hydroxide (98.9%; Merck), Tetraethyl orthosilicate (TEOS, > 99%, Sigma-Aldrich), 1-(2-hydroxyethyl)-3,3-dimethylindolino-6'-nitrobenzopyrylospiran (SPI; H1042; > 93%; TCI Chemicals), ethanol (95%; VWR) and HCl (37%; Labkem).

2.2 Synthesis of raw saponite

Raw saponite was prepared according to a previous methodology [40], having the ideal formula per half unit cell: $Na_{0.4}[(Si_{3.6}Al_{0.4})Mg_3O_{10}(OH, F)_2].nH_2O$. The precursor gel was obtained by reagent mixture added in the following order: deionized water (65.38 g; 3.63 mol),

hydrofluoric acid (0.38 g; 0.96 mmol), sodium acetate (0.18 g; 2.15 mmol), magnesium acetate (3.46 g; 16.14 mmol), aluminium oxide (0.34 g; 3.33 mmol) and silica (1.15 g; 19.21 mmol). The initial hydrogel presented the following chemical composition $1.00SiO_2$: $0.06Al_2O3$: $0.83MgO$: $0.06Na_2O$: $0.05HF$: $192.00H_2O$. It was kept under magnetic stirring at 25 °C for 4 h and then was transferred to an autoclave and heated at 220 °C for 72 h. Finally, the final solid was washed with deionized water, centrifuged, and dried at 50 °C for 48 h.

2.3 Synthesis of Al_2O_3 pillared saponite

Al_2O_3 pillared saponite was prepared according to an adapted procedure from Bergaoui *et al*. (1995) [41]. Initially, the aluminium pillaring solution was obtained by hydrolysing aluminium chloride with a NaOH solution up to OH:Al ratio of 2.2 and final concentration of Al^{3+} 0.1 mol L^{-1}. The solution was kept under magnetic stirring for 24 h at 25 °C and then added, dropwise, to the aqueous saponite suspension, resulting in a mixture of 7.5 mmol Al^{3+} per gram of clay. The mixture was aged under stirring for 24 h at room temperature. The obtained solid was centrifuged and washed with deionized water and dried at 50 °C for 24 h and then named as Sap-Al. Finally, the Sap-Al sample was calcined at 500 °C for 2 h and the final pillared saponite was designated as PilSap.

2.4 Preparation of the photosensible pigments

Two different preparations were used for the synthesis of the pigments. The first method was based on adsorption on the prepared solids and the second one was the in-situ hydrolysis of TEOS in presence of the dye. In both methods, the amount of SPI was 30 mg (0.085 mmol) for preparation of the hybrid pigments.

2.4.1 Preparation of the pigments by adsorption on Sap and PilSap

The adsorption of spiropyran on saponite and pillared saponite was carried out in acidic (pH 2) and basic (pH 13) media with predefined amounts of the solids for the preparation of the hybrid pigments as summarized in Table 1. The dye was initially solubilized in 2.5 mL of ethanol, then the solid was transferred to the dye solution and 2.5 mL of distilled water were added. pH of the medium was then adjusted by adding HCl 0.1 mol L^{-1} and NaOH 0.1 mol L^{-1}. All systems were stirred for 4 h and then the solids were separated by centrifugation, washed with ethanol, and dried at 50 °C for 24 h. Pigments were denominated considering mass (suffix 1 for 250 mg and suffix 2 for 1000 mg) and pH (A: acid; B: basic). A fixed amount of 250 mg was used in all preparations with the pillared saponite.

Table 1- Amounts of clay mineral samples used in the preparation of the hybrid pigments in acid and basic conditions.

Sample	Amount (mmol)	pH
Sap-SPI-A1	0.71	2
Sap-SPI-A2	2.83	2
PilSap-SPI-A	0.71	2
Sap-SPI-B1	0.71	13
Sap-SPI-B2	2.83	13
PilSap-SPI-B	0.71	13

2.4.2 Synthesis based on hydrolysis of TEOS

Pre-hydrolysis of TEOS was performed in 2.5 mL of water with specific amounts of silane, 12 and 24 mmol for TEOS-SPI-1 and TEOS-SPI-2 pigments, respectively. Pre-hydrolysis solution was kept under stirring for 24 h at 25 °C. Subsequently, SPI (0.085 mmol) dissolved in 3.2 mL of ethanol were added to the reactional medium. pH 2 was reached by

adding 0.1 mol L^{-1} HCl. The resulting gel was kept 24 h at 25 °C and dried at 50 °C without further separation between solid and solvent.

In addition, reference samples were prepared in the same conditions without use of spiropyrans and were denominated TEOS-1 (12 mmol TEOS) and TEOS-2 (24 mmol TEOS).

3. Characterizations

X-ray diffractograms were recorded using the D8 Advance Bruker-AXS diffractometer, with 30 kV, a current of 30 mA and CuKα radiation (λ = 1.5405 Å). The XRD patterns were obtained between 5-70° (2θ) with a scan rate of 0.5 degrees min^{-1}. The phase identification was performed using the DIFFRAC.EVA software. To better observe the (001) reflexion, 200 mg of the solids were dispersed in water (2 mL) and were kept under magnetic stirring for 30 minutes. Subsequently the mixture was deposited onto a glass slide and dried at 50 °C during 24 h and resulted in a film formation. The diffractograms were then collected under the same conditions as for the other samples. ^{27}Al NMR spectra were obtained on a Bruker Avance III spectrometer equipped with a 4 mm H-X MAS probe, operating at a frequency of 130.33 MHz. Calibration was performed using $Al(NO_3)_3$ (0 ppm) as an external standard.

^{13}C CP/MAS NMR spectra were obtained on a Bruker Advance 500 spectrometer operating at a frequency of 60.37 MHz. The proton cross polarization (CP-MAS) was applied with a contact time of 1 ms. The samples were rotated at the magic angle at a frequency of 10 kHz. The pulse length of ^{13}C was 5 ms (close to Π / 2) and the recycling delay was 3 s.

Thermogravimetric analyzes were performed using a TA Instrument SDT Q600 analyzer, with a heating rate of 10 °C min^{-1}, from 25 °C to 900 °C, under a dry air flow of 10 mL min^{-1} and using an alumina pan.

3.5 Test of the photoreversibility and UV-Vis diffuse reflectance

Test of the photoreversibility was performed by exposition of the pigments under a white light source for 2 h, using a 66 Klx intensity LED lamp. The pigments were characterized, before and after exposure to light, by diffuse reflectance spectrocolorimetry performed on an Ocean Optics modular spectrophotometer equipped with halogen and deuterium HL-2000-FHSA light source and incident light beam, with material made from the Ocean Optics USB4000 detector. For each acquisition, 30 scans were accumulated between 400 to 950 nm.

4 Results and discussion

4.1 X-Ray diffraction

XRD patterns of the raw and pillared saponites are presented in Figure 2. Typical reflections of the saponite were observed at 2θ values of 7.34° associated to a basal spacing of 1.21 nm of the saponite and [42] at 60.6° (d = 0.153 nm, 060 plan) corresponding to the trioctahedral structure of the clay mineral [43,44]. Other reflections at 2θ of 19.7°, 27.8°, 34.9° and 53.2° were typical of saponite. After pillarization, the (001) reflexion becomes too broad due probably to a heterogeneity in the stacking of the layers. [45–47]. The other reflections of the raw saponite were maintained in the pillared sample.

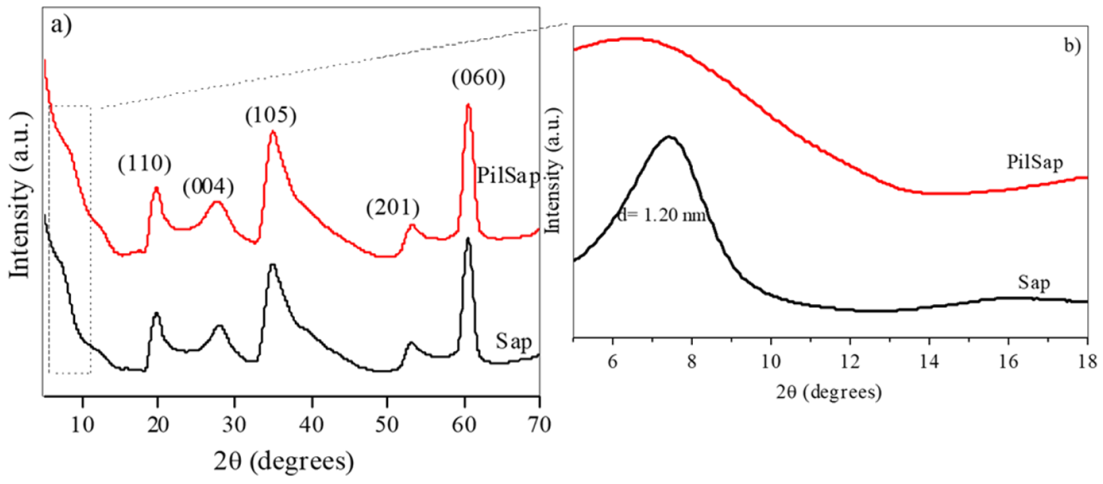

Figure 2 - X-ray diffractograms of saponite and pillared saponite (a) between 8° and 70° (2θ) and b) between 2° and 18° (2θ).

For the pigments prepared with saponite obtained in acidic and basic conditions, the basal spacings were 1.33 nm for Sap-SPI-A1 and 1.38 nm for Sap-SPI-B1 (Figure 3a). However, for the pigments obtained from the pillared saponite, pH influenced the adsorption. Intercalation of the SPI molecule into the interlayer space of the clay mineral, in acidic or basic medium, is not considered since the basal spacing (d_{001}) increased only from 1.37 nm to 1.44 nm in PilSap-SPI-A. In basic medium, phenolate species are present and induce a repulsion between the dye and the external surface of the clay.

The XRD results for the pigments obtained by TEOS hydrolysis reactions in acidic medium (Figure 3b) showed broader reflections [48] around 2θ 20-30° characteristics of amorphous silica with a certain degree of organization in the short and medium ranges [49,50]. The samples with SPI also presented an amorphous profile with two broad diffraction peaks at 2θ equal to 7.82° with spacing values of 1.12 nm and the similar at 2θ of 24.3°.

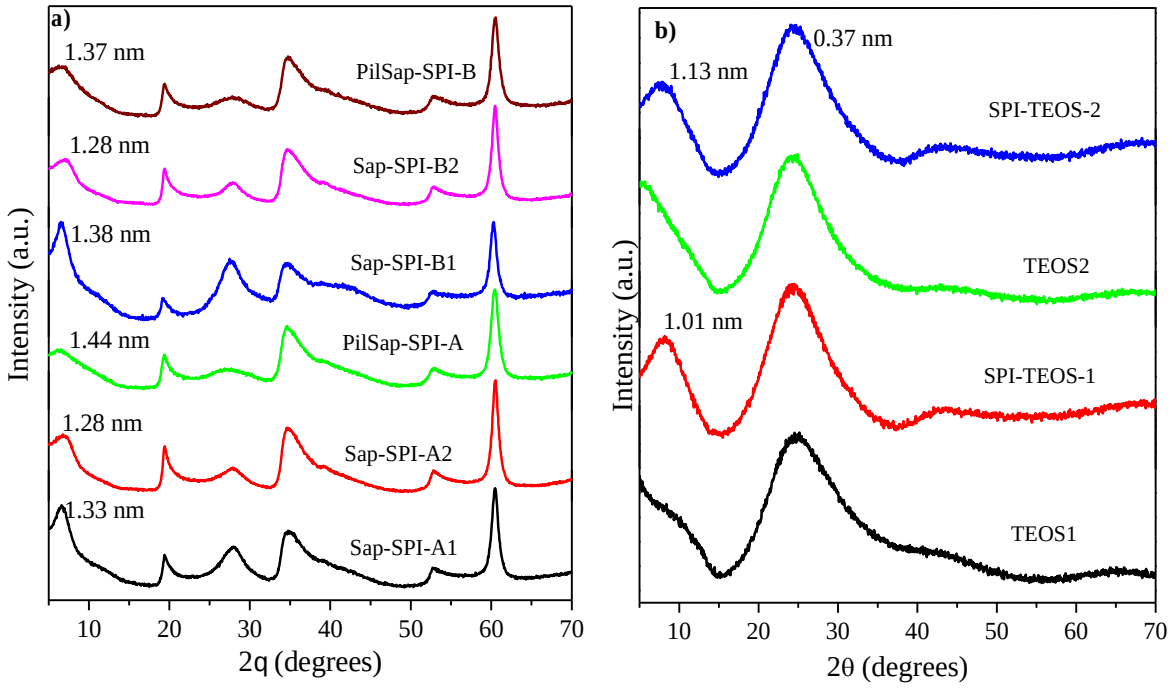

Figure 3 - X-ray diffractograms for samples derived from a) saponite and b) TEOS hydrolysis.

4.3 Solid state NMR

^{13}C CP/MAS NMR (Figure 5) was useful to confirm the presence of the dye in the pigments and help in the assignment of the interactions between dyes and solids. The SPI spectrum analysis considered the presence of the SP and MC isomeric structures in the dye molecule before and after adsorption and their assignments were based on studies of the free dyes [51,52]. Signals of geminal methyl groups were observed at 21.7 and 29.5 ppm for C19 and C20, respectively, furthermore, the lower frequency of C19 in relation to C20 is in agreement with the literature [52]. The signals of the aromatic carbons were in the region of 170-100 ppm as well as at 121 and 130 ppm related to unsaturated C8 and C7, respectively [51,52]. Moreover, characteristic signals of carbonyl groups were present in the region between 190-170 ppm (Figure 5b), these signals indicate the presence of the carbonylated MC isomeric form and suggest that part of the molecule SPI was in its neutral form. Influence of electronegativity of the atoms that decrease shielding of the carbon was also observed in the NMR spectra [53]. This effect causes shifts in signals, as observed at 162.3 ppm for C5, 149.8 ppm for C2 and C3', 143 ppm for C15 and 137.3 ppm for C5'. Other signals were also observed for C1 in 108.7 ppm, C17 in 47.5 ppm, C17' in 54.5 ppm and C18 in 63.3 ppm [52,54,55].

For the saponite sample containing spiropyran, the presence of signals related to C18 of the dye shifted from 63.3 ppm in SPI to 59.0 ppm in Sap-SPI-A1. From these results, it is reasonable the interaction between the dye and the saponite through hydrogen bonding between the OH groups of the SPI and the Si-OH, Si-O-Si and Al-OH structural groups of the clay. Similar interactions have been reported for other dyes when adsorbed on smectites [56]. On the other hand, ^{27}Al NMR spectra of the SAP-SPI-A sample did not show any significant changes in the aluminium environment (Figure 6). Thus, it is suggested hydrogen bonding only occurs

between a proton generated hydroxyl group of SPI and silanol groups or oxygen atom in the saponite surface [72]. The results are in close agreement to the XRD data.

For SPI-TEOS samples, ^{13}C CP/MAS NMR spectra presented more defined signals in the 170 to 100 ppm region, which is characteristic of unsaturated carbons and aromatic ring. The signals of carbonyl groups were observed between 190-170 ppm for SPI-TEOS-1. In addition, chemical displacement from 63.0 to 59.0 ppm and from 29.5 to 26.8 ppm were noticed for signals of the C18 and C20 in SPI, respectively. The observed variations are due to a better protection of the carbons, suggesting that the interaction of the dye with the polymeric gel also occurs though hydroxyl groups. Other peaks for the two solids were attributed to the residual ethoxy groups at 17.8 ppm (O-CH_2-CH_3) and 61.5 ppm (O-CH_2-CH_3) in ethanol [57,58].

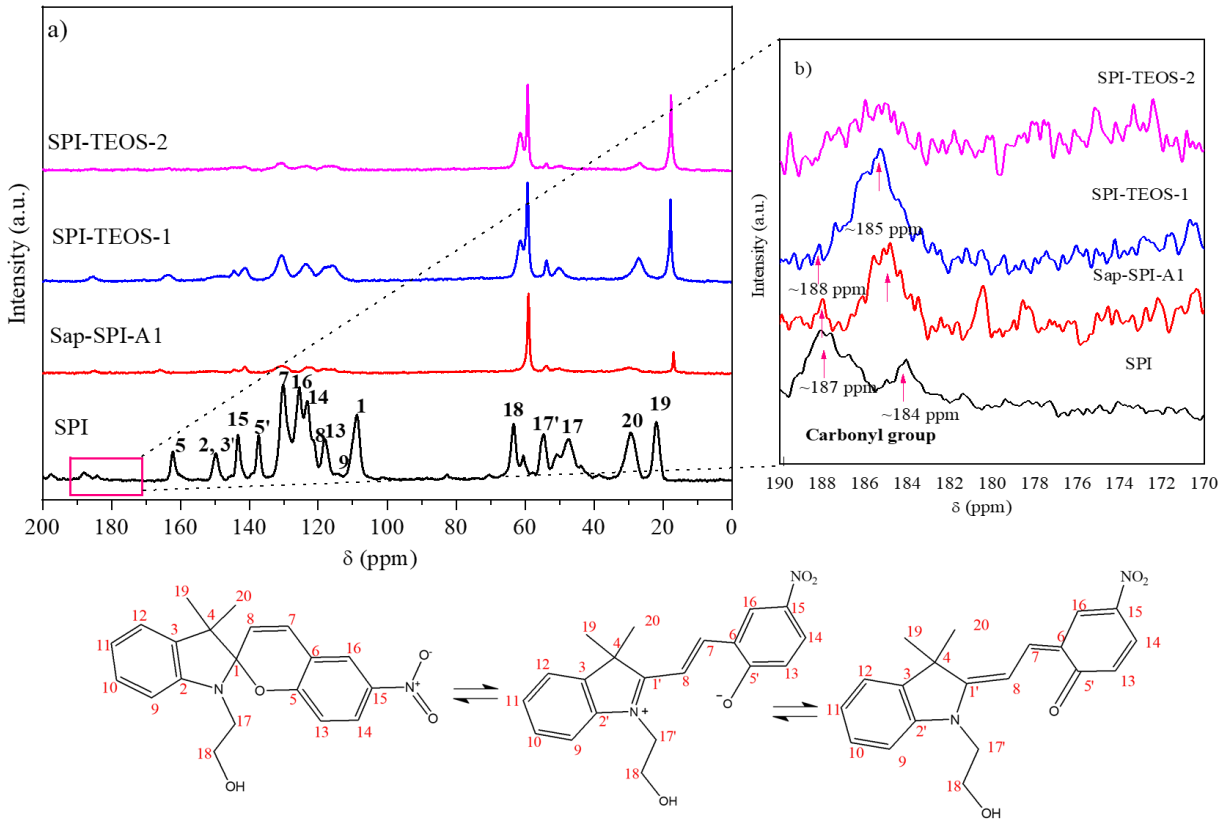

Figure 5 - ^{13}C CP/MAS NMR spectra for SPI and pigments obtained by adsorption ad TEOS hydrolysis: a) between 200-0 ppm and b) spectra increase between 190-170 ppm.

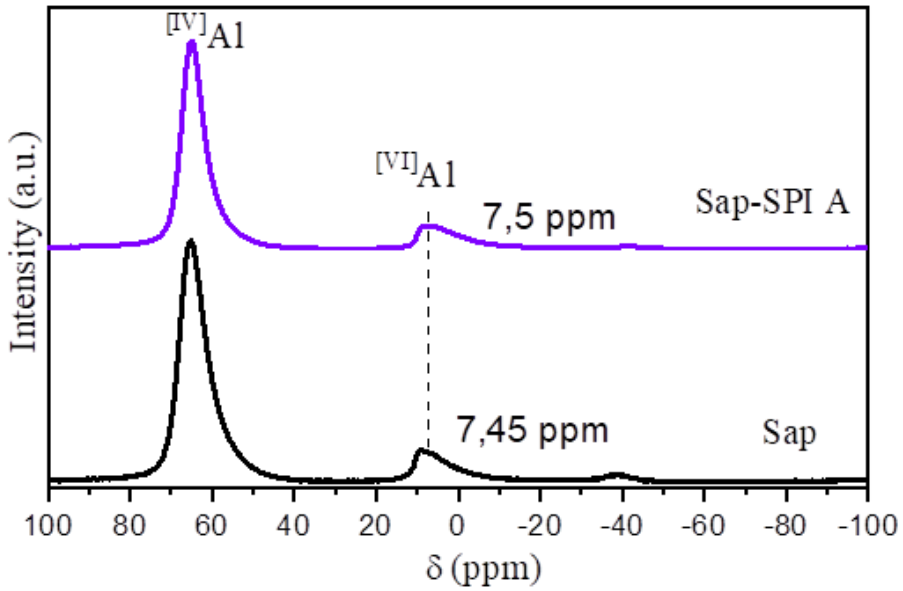

Figure 6 - ^{27}Al NMR spectra for precursor matrix and a hybrid pigment obtained by adsorption of spiropyran in saponite.

4.4 Thermal analysis

The thermal behavior of the prepared samples was investigated using TGA and DTA. All curves for the prepared pigments are presented in Figure 7-8 and the data are summarized in Table 2. Raw and pillared saponite presented three stages of mass loss [74]. During initial heating up to 250-280 °C, both matrices showed endothermic peaks at approximately 65 °C that corresponded to 9.3% and 5.4% of physiosorbed water for Sap and PilSap samples, respectively. The second event between 250-671 °C is associated to the interlayer water, reaching the mass losses around 2% for both samples. The third region up to 637-871 °C was attributed to the dehydroxylation of OH groups which corresponded to 3.4% and 2.9% for raw and pillared saponite, respectively [59, 74].

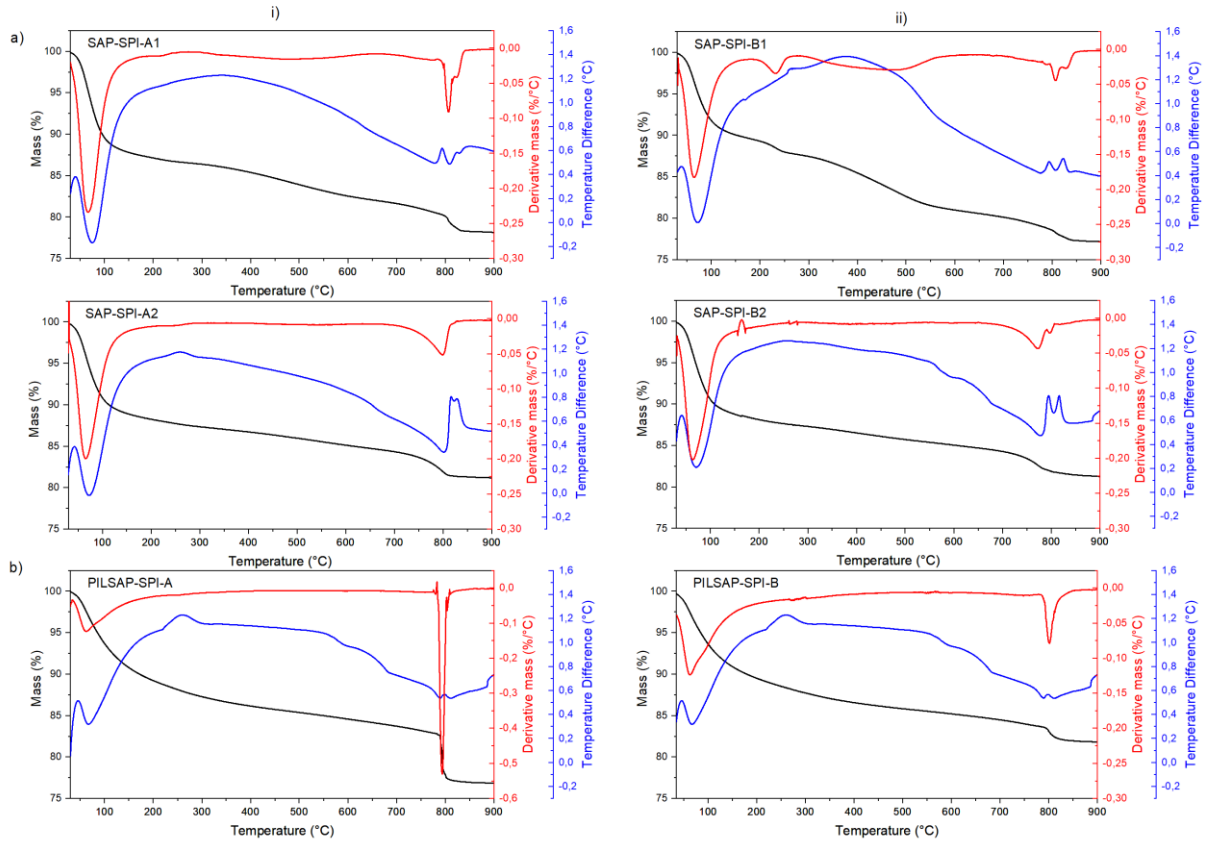

297

298 Figure 7 – TGA/DTG/TDA curves for the hybrid pigments prepared under i) acid and ii) basic

299 conditions and based on spiropyran adsorbed onto a) raw saponite and b) pillared saponite.

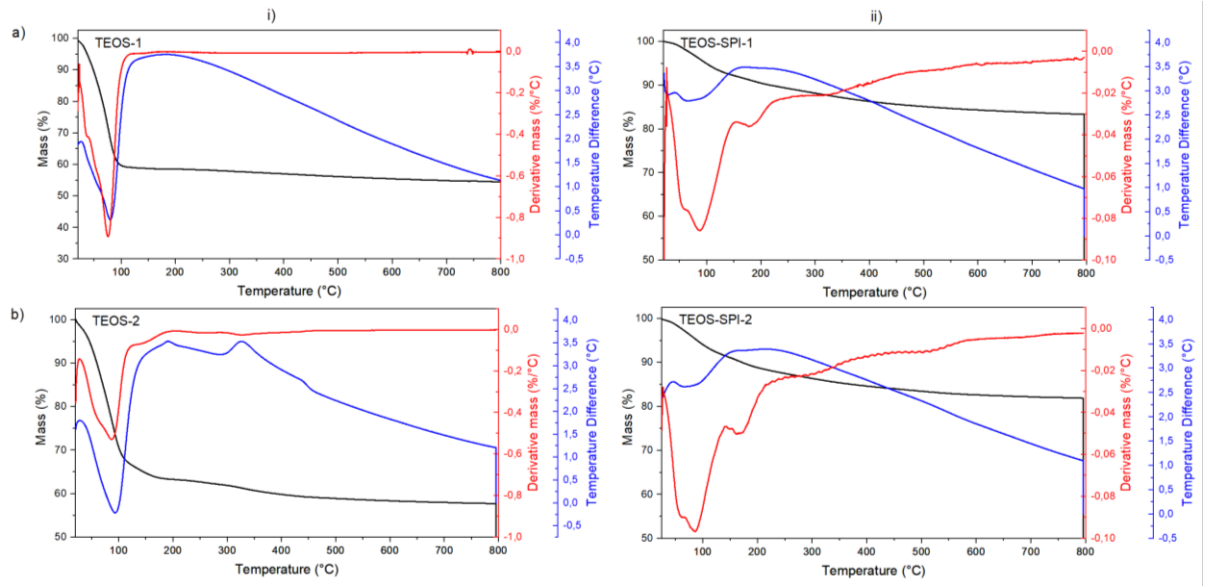

300

301 Figure 8 – TGA/DTG/DTA curves for i) raw samples and ii) hybrid pigments based on

302 spiropyran obtained by hydrolysis of a) 12 mmol and b) 24 mmol of TEOS.

303

304 Table 2 - Thermogravimetric data from the raw samples and hybrid pigments based on saponite,

305 pillared saponite and hydrolysis of TEOS containing a spiropyran dye.

Sample	Event	Temperature (°C)	Mass loss (%)	Total (%)
Sap	I	30-250	9.3	14.9
	II	250-637	2.2	
	III	637-845	3.4	
Sap-SPI-A1	I	30-187	12.6	21.6
	II	187-640	5.1	
	III	661-856	3.9	
Sap-SPI-A2	I	30-219	11.8	18.6
	II	219-673	3.5	
	III	673-852	3.3	
Sap-SPI-B1	I	30-175	10.2	22.7
	II	175-640	9.0	
	III	640-867	3.4	
Sap-SPI-B2	I	30-251	12.2	18.5
	II	251-645	2.9	
	III	645-867	3.4	
PilSap	I	30-280	5.4	8.3
	II	280-671	2.1	
	III	671-871	2.9	
PilSap-SPI-A	I	30-218	11.2	20.1
	II	218-781	6.0	
	III	781-857	2.9	
PilSap-SPI-B	I	30-220	10.9	19.1
	II	220-777	5.4	
	III	777-871	2.9	
TEOS-1	I	30-185	39.0	43.1
	II	185-800	4.1	
TEOS-2	I	30-129	32.2	40.7
	II	129-192	2.9	
	III	192-453	4.1	
	IV	453-800	1.5	
TEOS-SPI-1	I	30-155	7.7	16.4
	II	155-630	7.9	
	III	630-800	0.8	
TEOS-SPI-2	I	30-142	8.2	17.8
	II	142-225	2.4	
	III	225-460	5.2	
	IV	460-800	2.0	

Sap and PilSap-based pigments also presented three mass loss events (Figure 7). The first step of degradation up to 175-280 °C is assigned to the loss of physisorbed water and dehydration of interlayer cations with a mass loss around 10% for both raw SAP and PilSap-based pigments. Previous studies have shown that free spiropyran dye is stable until 180 °C, being decomposed around 250 °C [51,60]. Thus, the second event up to 640-781 °C is related to both decomposition of organic matter and dehydroxylation [51,60]. After dye loading, the mass losses associated to the second event increased to 5.1%, 3.5%, 9.0%, 2.9%, 2.1%, 6.0% and 5.4% for Sap-SPI-A1, Sap-SPI-A2, Sap-SPI-B1, Sap-SPI-B2, PilSap-SPI-A and PilSap-SPI-B samples, respectively. Lastly, the third event up to 856-871 °C is related to phase transition into enstatite. The results showed that loaded pillared samples did not show major differences in the mass loss associated to the dye (around 3%), once it was applied the same amount of clay matrix in the preparations. However, it is suggested that loaded saponite presented a high dye content in samples with low amount of the clay matrix. The best performance was observed for Sap-SPI-B1 sample, highlighting the loading under basic conditions.

For SiO_2 solids obtained from hydrolysis and polymerization of TEOS, two mass loss events were observed for TEOS-1, and four events for TEOS-2 samples (Figure 8). The first event was attributed to the elimination of adsorbed water on the silica surface. The weight loss decreased rapidly to 39% and 32% with endothermic peaks at 110 °C and 123 °C for TEOS-1 and TEOS-2, respectively. The second event in TEOS-1 (mass loss of 4.1%) which is probably related to the degradation of the remaining organic matter due to incomplete TEOS hydrolysis and condensation, and to the residual -OH groups on the surface of the silica. [61,62]. It seems that a high amount of TEOS promoted a different polymerization in TEOS-2 samples. Its second stage of decay occurred between 129 °C and 192 ºC and can be ascribed to the trapped

water molecules between silica particles or into the network structure. The third event (mass loss of 4.1%) is associated to the organic matter from the incomplete hydrolysis of alkoxide TEOS, whereas the last one (mass loss of 1.5%) related to the residual -OH groups on the surface of the silica [61,62]. All mass losses observed for the matrices prepared by hydrolysis of TEOS were accompanied by an endothermic transformation.

TGA/DTA curves of pigments based on TEOS showed two stages of mass loss for TEOS-1 and four events for TEOS-2 sample (Figure 8). A decrease in the mass loss related to dehydration on the first stage of both samples (7.7% for TEOS-SPI-1 and 8.2% for TEOS-SPI-2) and an increase of the mass loss in the 2^{nd} and 3^{rd} regions for TEOS-SPI-1 and TEOS-SPI-2 samples, respectively, highlighted the load of spiropyran dye with a high content for TEOS-SPI-1 sample. In addition, the dye mass loss occurred from 185-225 °C, simultaneously with the remaining organic matter from the incomplete TEOS hydrolysis.

4.5 UV-VIS diffuse reflectance and photochromism test

The selected pigments were evaluated by photochromism test and UV-VIS diffuse reflectance spectra were collected before and after the exposure period, as well as in dark condition. Qualitatively, significant color variations were observed for the samples (Figure 9). After test in dark, it was also observed that Sap-SPI-B did not show a color reversibility in the same proportions as occurred for the other samples. This fact probably indicates that in basic medium, the formed pigments have a lower reversibility potential than those formed in acidic medium. On the other hand, the pigments formed by hydrolysis showed more intense colors than the initial solids.

Figure 9 – Photochromism assay for pigments of spiropyran.

The UV-VIS diffuse reflectance spectra showed different characteristics for each sample. This fact was related to the color variation of the spiropyran, due to the change in ionization induced by the pH of the medium. The SPI spectrum in Figure 10 presented two bands in the 500-600 nm region attributed to the merocyanine (MC) zwitterionic form [7]. Similar spectral profiles have been observed for spiro compounds in nonpolar solutions [67-69]. The planar structure with a prolonged π conjugation between the indoline and chromene portions in the CM, presents a delocalized transition that changes in visible region in relation to closed ring isomer. On the other hand, the spiropyran (SP) form presented two localized transitions at 295 nm and 294 nm assigned to the π-π* electronic transition of the indoline and the chromene moieties, respectively [67,70,71]. Such understanding allows the differentiation of the isomeric form present in the prepared systems by the analysis of the spectrum and a better understanding of the possible interactions between dye and host matrices.

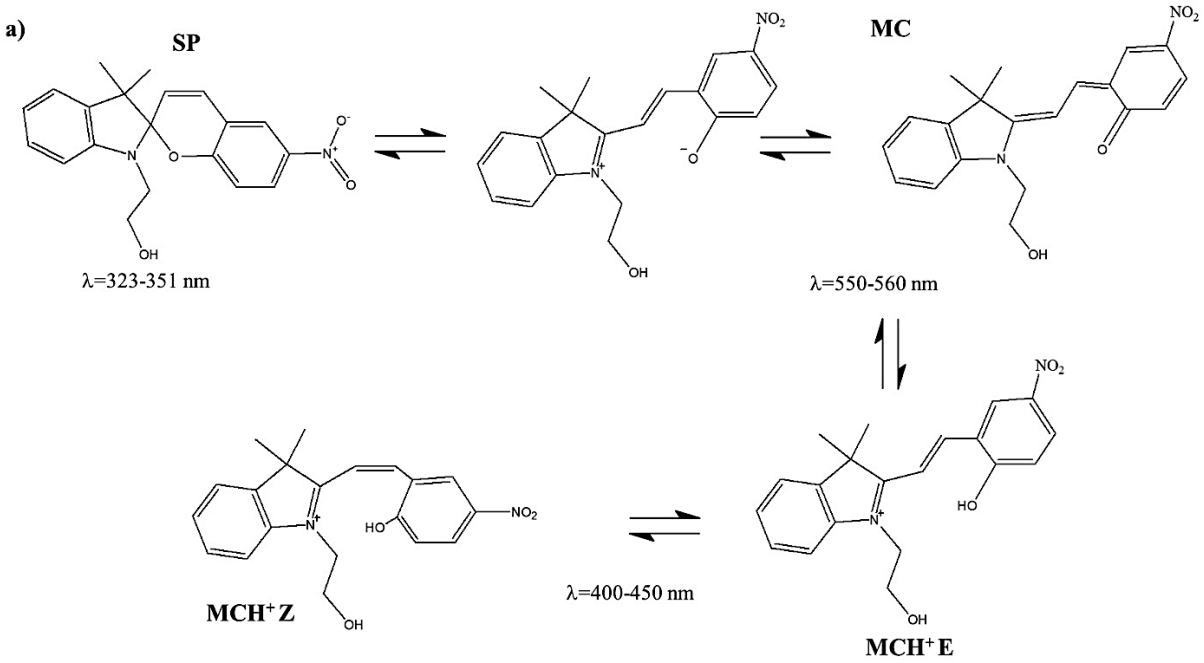

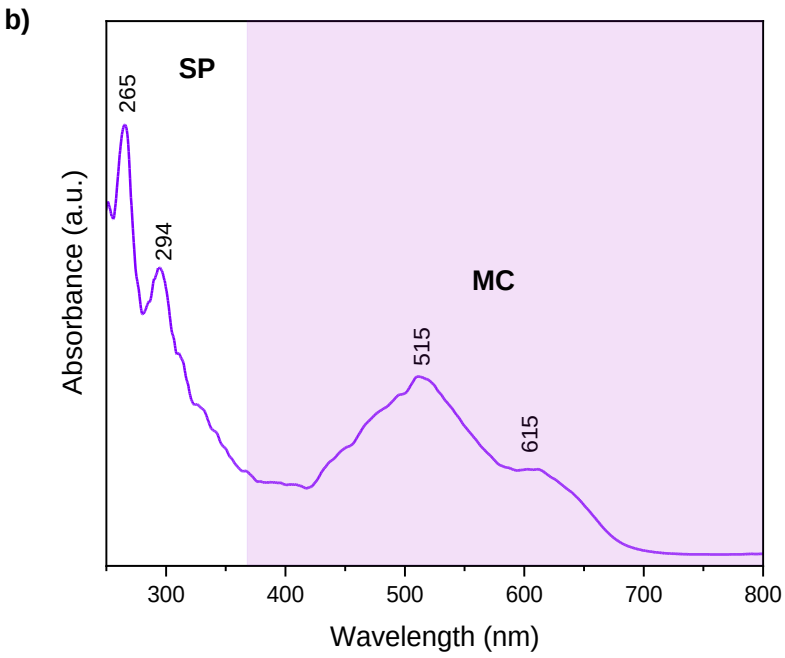

Figure 10 – SPI H1042 a) isomeric forms and b) UV-Vis absorption spectra.

All prepared pigments presented two characteristic absorption bands around 450-550 nm (Figure 11). The first absorption band in the pigments based on saponite and pillared saponite (Figure 11i-iv) at 440 nm was attributed to the MCH^+ form and the second at 560 nm, observed for the four samples may be correlated to the zwitterionic form [55,63]. After reversibility test, the samples obtained in acidic medium presented a broad band centered around 450 nm,

suggesting the conversion of the isomeric forms with a predomination of the MCH^+ form. In contrast, samples prepared under basic conditions have presented minor spectral variations after 24 h in the dark.

The pigments prepared by TEOS hydrolysis (Figure 11v-vi) exhibited a broad band centered at 500 nm which can be attributed to the predominance of the zwitterionic form [7]. Both samples presented some color reversibility, highlighting the effect of the acidic medium for the photoreversible systems.

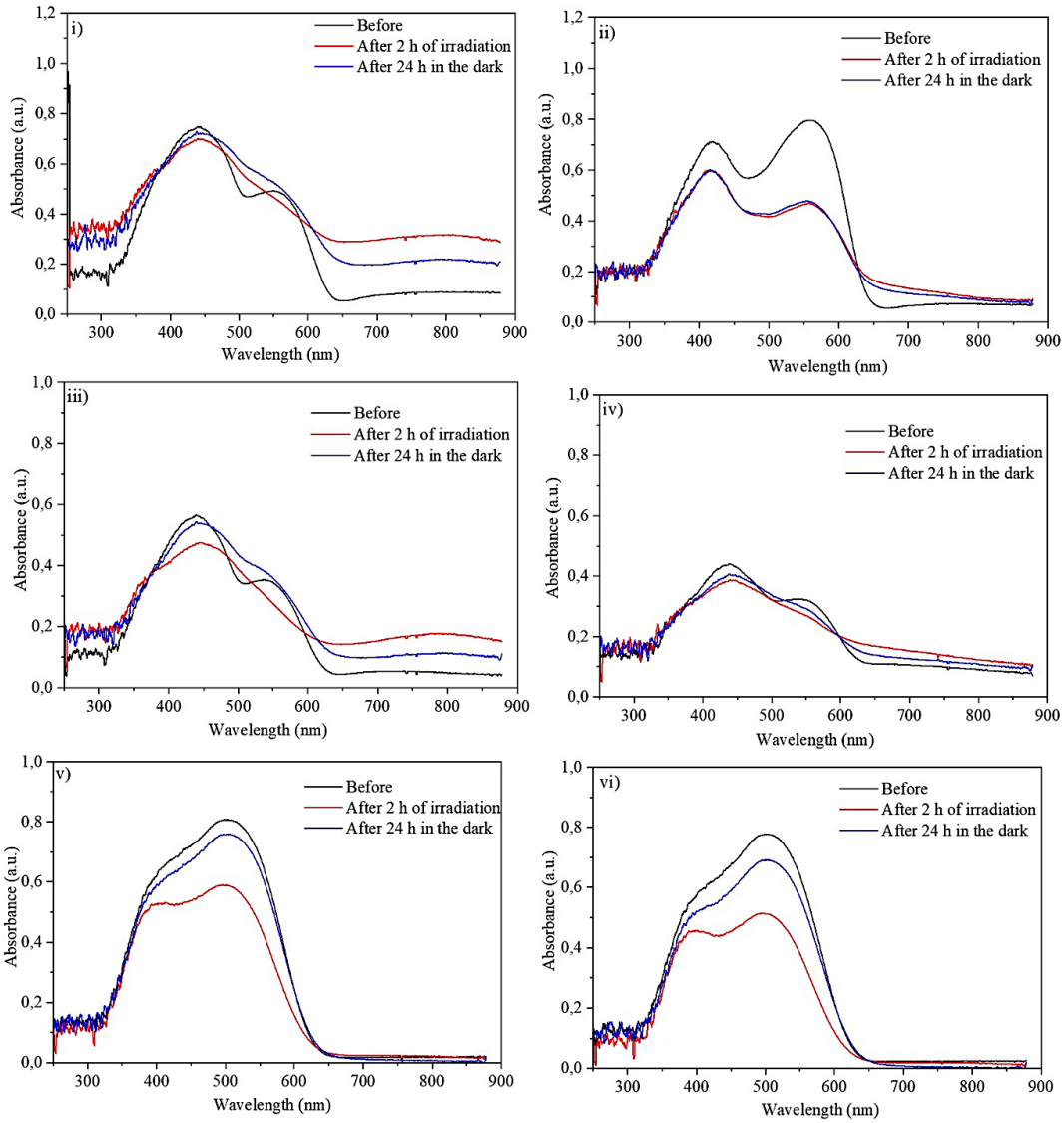

Figure 11- UV-Vis spectra for pigments before and after photochromism tests: i) Sap-SPI-A2; ii) Sap-SPI-B2; iii) PilSap-SPI-A; iv) PilSap-SPI-B; v) SPI-TEOS-1 and vi) SPI-TEOS-2.

All pigments presented a decrease in the bands intensity after light exposure, especially in the region of 400 nm. SPI-TEOS-1 and SPI-TEOS-2 samples. The spectra obtained for the samples after 24 h in the dark presented similar profiles to the initial samples. Except for the Sap-SPI-B2 sample, minor color difference was observed for the samples before and after light exposure. The results suggested the prepared pigments presented photostability with a regeneration capacity after light exposure and subsequent time-out in the dark.

4.6 Influence of the pH and isomeric changes

Color variations observed for the prepared hybrid pigments can be explained by the speciation of the SPI dye and the surface charge of the mineral surface which are pH dependent. Regarding clay particles, the literature indicates that their edges are positively charged at pH below 7, although some data suggest they are already neutralized at pH 6 [72]. On the other hand, the surface is negatively charged with the increase of pH values above that. Therefore, it is expected that saponite and pillared saponite exhibited a positive net charge at very low pH such at pH 2, applied in our experiments. Likewise, a negative net charge is expected for these surfaces at very high pH i.e.13, applied in our experiments.

In its turn, some spiropyran compounds have chromic acid, and the isomeric variation depends on a favorable medium for the molecular planarization. The polar merocyanine form (MC) is then stabilized in relation to the spiropyran (SP) form when in presence of protons [7,12]. In its zwitterionic form (MC), negatively charged phenolate oxygen can bind to metal cations in an optically controlled reversible process [55]. In addition to complexation with cations, phenolate anion can be protonated, where the molecule shows the MCH^+ form which is detected in the absorption spectrum at 400-450 nm, while the MC isomer at 500-600 nm [7,13,55,63]. The process can also be followed qualitatively, via color variation from purple (MC) to yellow (MCH^+) after protonation, as observed in Figure 12 [64].

412

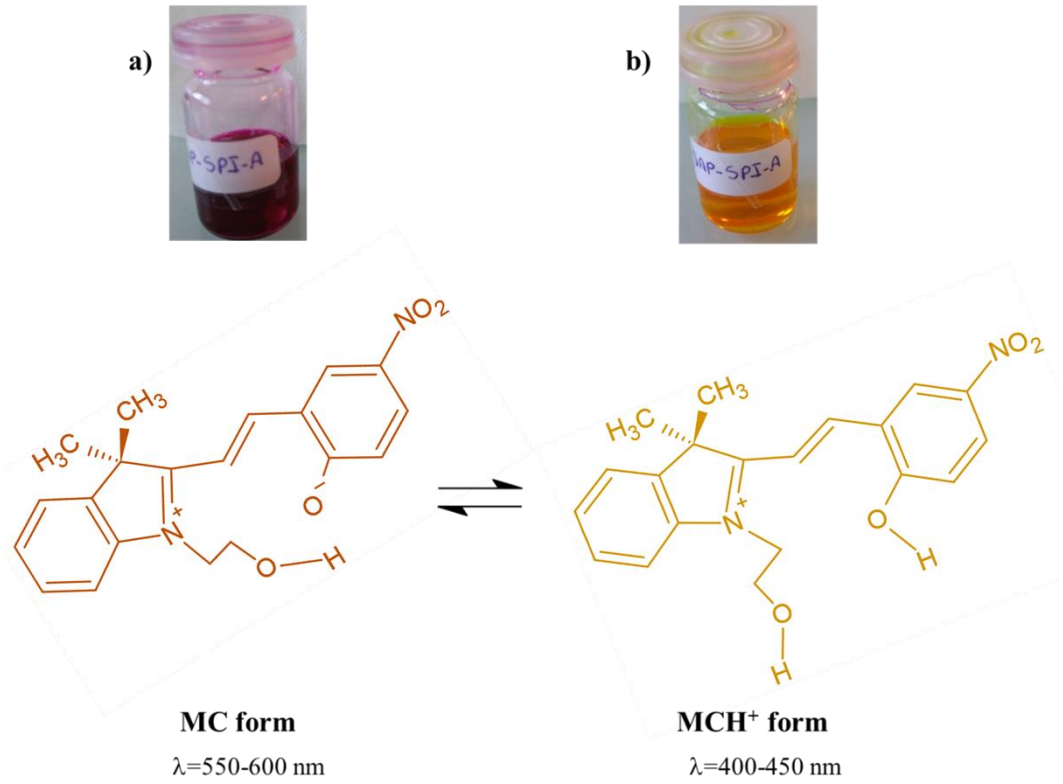

413

414 Figure 12 - Illustration of the SPI H1042 isomeric forms a) MC and b) MCH^+ in acidic solution.

415 UV-Vis data of the prepared pigments have suggested that the MCH^+ and MC isomeric
416 SPI forms are stabilized in the proposed silica-based matrices. Based on predicted pKa = 14.46
417 ± 0.10 for H1042 molecule, MC form is partially deprotonated at the pH 13 and is predominant
418 in experiments under basic conditions. Likewise, MCH^+ species are dominant in pigments
419 prepared under acid conditions. From XRD data it is not evidenced intercalation for the saponite
420 based samples. Moreover ^{13}C and ^{27}Al NMR data have suggested that interactions occur
421 through hydrogen bonding between hydroxyl groups of SPI and silanol groups in the saponite
422 matrix. In addition, intramolecular hydrogen bonding between proton in hydroxyl groups and
423 O− generated by cleavage of spirocarbon−oxygen bond is also expected to MC form [73]. Thus,
424 the following interaction mechanism for the SPI species in the saponite-based pigments is
425 proposed in Figure 13, considering both MC and MCH^+ isomeric forms of H1042 spiropyran.

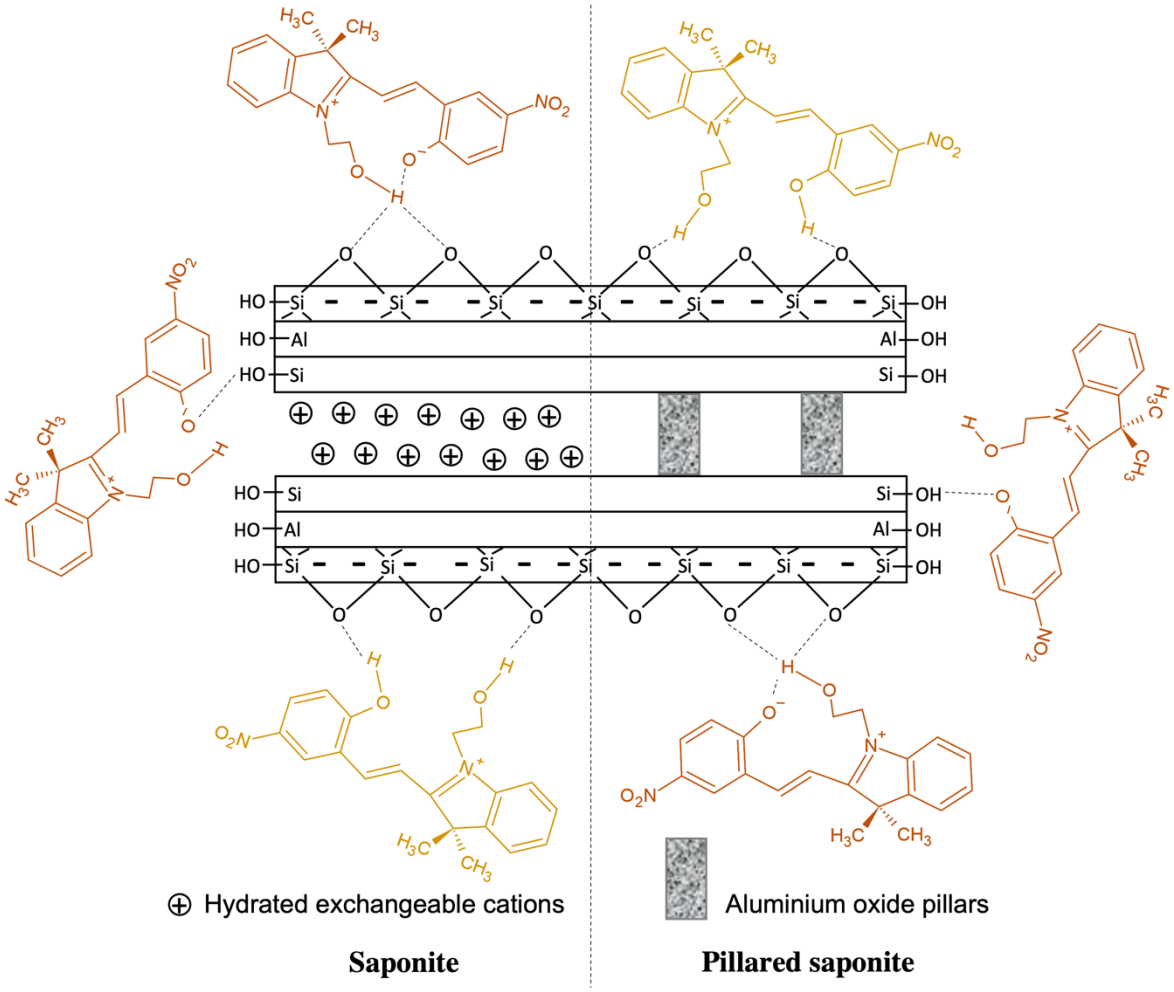

Figure 13 – Interaction mechanism of the spiropyran species in the saponite-based pigments.

Protonated merocyanine interaction with silanol groups of the host matrix through hydrogen bonds is favored under acid conditions. On the other hand, MC form interacting with oxygen atoms of the Si-O-Si structural groups of the saponite is dominant under basic conditions. However, both situations are present in all saponite-based pigments and their color variations are related to the isomeric forms content adsorbed onto the matrices. In basic medium, the presence of the phenolate species can generate certain repulsion between the dye and the layers of the matrix. This effect resulted in less stable pigments than those obtained in acidic medium. Furthermore, the interaction from silanol groups may promoted steric effects, impairing intercalation in both pH systems.

Analogous to the saponite-based samples prepared under acid conditions, the pigments from the hydrolysis of TEOS presented the predominance of the protonated MC form and the presence of hydrogen bonding as the principal mechanism of dye/silica interaction.

5.0 Conclusion

Hybrid photochromic pigments were prepared by adsorption of 1'-(2-hidroxietil)-3',3'-dimetil-6-nitrospiro[1(2H)-benzopirano-2,2'-indoline] on raw and pillared saponites, and by coprecipitation in the presence of hydrolyzed TEOS. The obtained solids were characterized by X-Ray diffraction, ^{13}C CP/MAS NMR and thermogravimetry. The color stability of the prepared pigments was evaluated before and after light exposure. Characterization results suggested incorporation of the dye via hydrogen bonding as the principal mechanism of interaction in the pigments. Thermal analysis data indicated that the pigment based on raw saponite with low amount of the clay matrix under basic condition contain a high dye content than those based on pillared saponite under acid condition. The absence of SP bands in the UV-VIS spectra suggested the silica-based matrices stabilized SPI in the MCH^+ and MC isomeric forms. In addition, the incorporation of the dye in the host silica-based matrices was pH dependent with protonated merocyanine species dominant at pH 2 and zwitterionic merocyanine as major species at pH 13. Regarding the colors, the prepared pigments showed a custom color palette between purple and yellow dependent on the dominant SPI isomeric forms with relative stability after light irradiation. All prepared pigments presented relative photoreversible capacity after recovery at 24 h in the dark. The finds of this study propose the multicolored prepared hybrids as promising materials to be applied in photochromic systems as smart pigments.

Acknowledgements

We acknowledge the financial support from the CAPES/COFEBUB (Project n° 835/15) and FAPESQ-PB (Project n° 027/2018). The authors thank Île-de-France region and CNRS for funding.

References

[1] Ercole F, Davis TP, Evans RA. Photo-responsive systems and biomaterials: Photochromic polymers, light-triggered self-assembly, surface modification, fluorescence modulation and beyond. Polym Chem 2010;1:37–54. https://doi.org/10.1039/b9py00300b.

[2] Lakmali UGR, Hettiarachchi C V. Pseudo crystalline state thermochromic and reverse-photochromic reactivity of spiroindolinobenzopyran upon encapsulation into Zn-MOF-74. CrystEngComm 2015;17:8607–8611. https://doi.org/10.1039/C5CE01639H.

[3] P. Bamfield. Chromic Phenomena : Technological Applications of Colour Chemistry Royal Society of Chemistry. R Soc Chem 2010. https://doi.org/10.1039/c3ra43922d.

[4] Funasako Y, Okada H, Inokuchi M. Photochromic Ionic Liquids Containing Cationic Spiropyran. vol. 3. 2018. https://doi.org/10.1002/cptc.201800197.

[5] Irie M, Fukaminato T, Matsuda K, Kobatake S. Photochromism of Diarylethene Molecules and Crystals: Memories, Switches, and Actuators. Chem Rev 2014;114:12174–277. https://doi.org/10.1021/cr500249p.

[6] Seeboth A, Lötzsch D, Ruhmann R. First example of a non-toxic thermochromic polymer material-based on a novel mechanism. J Mater Chem C 2013;1:2811–6. https://doi.org/10.1039/c3tc30094c.

[7] Klajn R. Spiropyran-based dynamic materials. Chem Soc Rev 2014;43:148–84. https://doi.org/10.1039/c3cs60181a.

[8] Cheng Y, Zhang X, Fang C, Chen J, Wang Z. Discoloration mechanism, structures and recent applications of thermochromic materials via different methods: A review. J Mater Sci Technol 2018;34:2225–34. https://doi.org/10.1016/j.jmst.2018.05.016.

[9] Lee CY, Hu CH, Cheng SL, Chu CC, Hsiao VKS. Reversible photoluminescence in spiropyran-modified porous silicon. J Lumin 2014;159:246–50. https://doi.org/10.1016/j.jlumin.2014.11.021.

[10] Xu Z, Li S, Shen Y, Chen M, Shao X. Spiropyran-azobenzene-DBU system as solvent indicator. Tetrahedron Lett 2018;59:3829–32. https://doi.org/10.1016/j.tetlet.2018.07.025.

[11] Radu A, Byrne R, Alhashimy N, Fusaro M, Scarmagnani S, Diamond D. Spiropyran-based reversible, light-modulated sensing with reduced photofatigue. J Photochem Photobiol A Chem 2009;206:109–15. https://doi.org/10.1016/j.jphotochem.2009.05.022.

[12] Florea L, Hennart A, Diamond D, Benito-Lopez F. Synthesis and characterisation of spiropyran-polymer brushes in micro-capillaries: Towards an integrated optical sensor for continuous flow analysis. Sensors Actuators, B Chem 2012;175:92–9. https://doi.org/10.1016/j.snb.2011.12.055.

[13] Teepakakorn A, Yamaguchi T, Ogawa M. The improved stability of molecular guests by the confinement into nanospaces. Chem Lett 2019;48:398–409. https://doi.org/10.1246/cl.181026.

[14] Sanchez C, Julián B, Belleville P, Popall M. Applications of hybrid organic-inorganic nanocomposites. J Mater Chem 2005;15:3559–92. https://doi.org/10.1039/b509097k.

505 [15] B. S. Lukyanov and M. B. Lukyanova. Spiropyrans: synthesis, properties, and
506 application. (review). Chem Heterocycl Compd 2005;41:1–31.

507 [16] Cao L, Fei X, Zhao H, Gu Y. Inorganic-organic hybrid pigment fabricated in the
508 preparation process of organic pigment : Preparation and characterization. Dye Pigment
509 2015;119:75–83. https://doi.org/10.1016/j.dyepig.2015.03.020.

510 [17] Hakeim OA, Arafa AA, Zahran MK, Abdou LAW. UV-curable encapsulation of
511 surface-Modified organic pigments for inkjet printing of textiles. Colloids Surfaces A
512 Physicochem Eng Asp 2014;447:172–82. https://doi.org/10.1016/j.colsurfa.2014.01.075.

513 [18] Fu S, Xu C, Du C, Tian A, Zhang M. Encapsulation of C.I. Pigment blue 15:3 using a
514 polymerizable dispersant via emulsion polymerization. Colloids Surfaces A Physicochem Eng
515 Asp 2011;384:68–74. https://doi.org/10.1016/j.colsurfa.2011.03.009.

516 [19] Ma ZL, Wei HM, Li CC, Yang PF. Silica sol-gel anchoring on aluminum pigments
517 surface for corrosion protection based on aluminum oxidized by copper ammonia complex ion.
518 Dye Pigment 2015;113:730–6. https://doi.org/10.1016/j.dyepig.2014.10.012.

519 [20] dos Santos C, Brum LFW, de Fátima Vasconcelos R, Velho SK, dos Santos JHZ. Color
520 and fastness of natural dyes encapsulated by a sol-gel process for dyeing natural and synthetic
521 fibers. J Sol-Gel Sci Technol 2018;86:351–64. https://doi.org/10.1007/s10971-018-4631-0.

522 [21] Švara Fabjan E, Otoničar M, Gaberšček M, Sever Škapin A. Surface protection of an
523 organic pigment based on a modification using a mixed-micelle system. Dye Pigment
524 2016;127:100–9. https://doi.org/10.1016/j.dyepig.2015.12.016.

525 [22] Morimoto K, Tamura K, Iyi N, Ye J, Yamada H. Adsorption and photodegradation
526 properties of anionic dyes by layered double hydroxides. J Phys Chem Solids 2011;72:1037–

527 45. https://doi.org/10.1016/j.jpcs.2011.05.018.

528 [23] Samuei S, Rad FA, Rezvani Z. The influence of intercalated dye molecules shape and
529 features on photostability and thermal stability between LDH layers. Appl Clay Sci
530 2020;184:105388. https://doi.org/10.1016/j.clay.2019.105388.

531 [24] Ribeiro HL, Oliveira AV de, Brito ES d., Ribeiro PRV, Souza Filho M de sá M, Azeredo
532 HMC. Stabilizing effect of montmorillonite on acerola juice anthocyanins. Food Chem
533 2018;245:966–73. https://doi.org/10.1016/j.foodchem.2017.11.076.

534 [25] De Queiroga LNF, França DB, Rodrigues F, Santos IMG, Fonseca MG, Jaber M.
535 Functionalized bentonites for dye adsorption: Depollution and production of new pigments. J
536 Environ Chem Eng 2019;7:103333. https://doi.org/10.1016/j.jece.2019.103333.

537 [26] Micó-Vicent B, Martínez-Verdú FM, Novikov A, Stavitskaya A, Vinokurov V, Rozhina
538 E, et al. Stabilized Dye–Pigment Formulations with Platy and Tubular Nanoclays. Adv Funct
539 Mater 2018;28:1–9. https://doi.org/10.1002/adfm.201703553.

540 [27] Silva GTM, Silva CP, Gehlen MH, Oake J, Bohne C, Quina FH. Organic/inorganic
541 hybrid pigments from flavylium cations and palygorskite. Appl Clay Sci 2018;162:478–86.
542 https://doi.org/10.1016/j.clay.2018.07.002.

543 [28] Chen H, Zhang Z, Zhuang G, Jiang R. A new method to prepare ‘Maya red’ pigment
544 from sepiolite and Basic red 46. Appl Clay Sci 2019;174:38–46.
545 https://doi.org/10.1016/j.clay.2019.03.023.

546 [29] Lu Y, Dong W, Wang W, Ding J, Wang Q, Hui A, et al. Optimal Synthesis of
547 Environment-Friendly Iron Red Pigment from Natural Nanostructured Clay Minerals.
548 Nanomaterials 2018;8:925. https://doi.org/10.3390/nano8110925.

549 [30] Mahmoodi A, Ebrahimi M, Khosravi A, Eivaz Mohammadloo H. A hybrid dye-clay
550 nano-pigment: Synthesis, characterization and application in organic coatings. Dye Pigment
551 2017;147:234–40. https://doi.org/10.1016/j.dyepig.2017.08.009.

552 [31] Aranda P, Detellier C. Beyond smectite-based nanocomposites. Appl Clay Sci
553 2016;130:18–9. https://doi.org/10.1016/j.clay.2016.06.021.

554 [32] Steger S, Stege H, Bretz S, Hahn O. A complementary spectroscopic approach for the
555 non-invasive in-situ identification of synthetic organic pigments in modern reverse paintings
556 on glass (1913–1946). J Cult Herit 2019:1–9. https://doi.org/10.1016/j.culher.2019.01.011.

557 [33] Zhu MQ, Zhang GF, Li C, Aldred MP, Chang E, Drezek RA, et al. Reversible two-
558 photon photoswitching and two-photon imaging of immunofunctionalized nanoparticles
559 targeted to cancer cells. J Am Chem Soc 2011;133:365–72. https://doi.org/10.1021/ja106895k.

560 [34] Chan YH, Gallina ME, Zhang X, Wu IC, Jin Y, Sun W, et al. Reversible photoswitching
561 of spiropyran-conjugated semiconducting polymer dots. Anal Chem 2012;84:9431–8.
562 https://doi.org/10.1021/ac302245t.

563 [35] Pardo R, Zayat M, Levy D. Hybrid materials themed issue Photochromic organic –
564 inorganic hybrid materials w 2011. https://doi.org/10.1039/c0cs00065e.

565 [36] Feeney MJ, Thomas SW. Tuning the Negative Photochromism of Water-Soluble
566 Spiropyran Polymers. Macromolecules 2018;51:8027–37.
567 https://doi.org/10.1021/acs.macromol.8b01915.

568 [37] Li M, Zhang Q, Zhou YN, Zhu S. Let spiropyran help polymers feel force! Prog Polym
569 Sci 2018;79:26–39. https://doi.org/10.1016/j.progpolymsci.2017.11.001.

570 [38] Kinashi K, Suzuki T, Yasunaga H, Tsuchida H, Sakai W, Tsutsumi N, et al. Carrier-

assisted dyeing of poly(L-lactic acid) fibers with dispersed photochromic spiropyran dyes. Dye Pigment 2017;145:444–50. https://doi.org/10.1016/j.dyepig.2017.06.040.

[39] Neugebauer W, Sessa C, Steuer C, Allscher T, Stege H. Naphthol Green – a forgotten artists' pigment of the early 20th century. History, chemistry and analytical identification. J Cult Herit 2019;36:153–65. https://doi.org/10.1016/j.culher.2018.08.008.

[40] Jaber M, Brendlé J. Influence du milieu de synthèse sur la cristallisation de saponite: proposition de mécanisme réactionnel en milieux acide et basique. vol. 8. Comptes. 2005. https://doi.org/10.1016/j.crci.2004.10.025.

[41] Bergaoui L, Jean-Franqois Lambert RF and HS. AI-Pillared Saponites Part 3.7'-Effect of Parent Clay Layer Charge on the Intercalation-Pillaring Mechanism and Structural Properties. J CHEM SOC FARADAY TRANS 1995;91:2229–39.

[42] Tangaraj V, Janot J-M, Jaber M, Bechelany M, Balme S. Adsorption and photophysical properties of fluorescent dyes over montmorillonite and saponite modified by surfactant. Chemosphere 2017;184:1355–61. https://doi.org/10.1016/j.chemosphere.2017.06.126.

[43] Bisio C, Gatti G, Boccaleri E, Marchese L, Superti GB, Pastore HO, et al. Understanding physico-chemical properties of saponite synthetic clays. Microporous Mesoporous Mater 2008;107:90–101. https://doi.org/10.1016/j.micromeso.2007.05.038.

[44] Jaber M, Miéhé-Brendlé J. Influence du milieu de synthése sur la cristallisation de saponite: Proposition de mécanisme réactionnel en milieux acide et basique. Comptes Rendus Chim 2005;8:229–34. https://doi.org/10.1016/j.crci.2004.10.025.

[45] Bergaya F, Theng BKG, Lagaly G. Pillared Clays and Clay Minerals. vol. 5. 2nd ed. Elsevier Ltd.; 2013. https://doi.org/10.1016/B978-0-08-098258-8.09992-2.

593 [46] Figueras F. Pillared Clays as Catalysts. Catal Rev 1988;30:457–99.
594 https://doi.org/10.1080/01614948808080811.

595 [47] Bertella F, Pergher SBC. Pillaring of bentonite clay with Al and Co. Microporous
596 Mesoporous Mater 2015;201:116–23. https://doi.org/10.1016/j.micromeso.2014.09.013.

597 [48] Ferreira-Neto EP, Ullah S, De Carvalho FLS, De Souza AL, De Oliveira M, Schneider
598 JF, et al. Preparation, characterization and photochromic behavior of phosphotungstic acid-
599 ormosil nanocomposites. Mater Chem Phys 2015;153:410–21.
600 https://doi.org/10.1016/j.matchemphys.2015.01.035.

601 [49] Šurca Vuk A, Fir M, Ješe R, Vilčnik A, Orel B. Structural studies of sol-gel
602 urea/polydimethylsiloxane barrier coatings and improvement of their corrosion inhibition by
603 addition of various alkoxysilanes. Prog Org Coatings 2008;63:123–32.
604 https://doi.org/10.1016/j.porgcoat.2008.04.018.

605 [50] Rios X, Moriones P, Echeverría JC, Luquin A, Laguna M, Garrido JJ. Ethyl group as
606 matrix modifier and inducer of ordered domains in hybrid xerogels synthesised in acidic media
607 using ethyltriethoxysilane (ETEOS) and tetraethoxysilane (TEOS) as precursors. Mater Chem
608 Phys 2013;141:166–74. https://doi.org/10.1016/j.matchemphys.2013.04.042.

609 [51] Gerkman MA, Yuan S, Duan P, Taufan J, Schmidt-Rohr K, Han GGD. Phase transition
610 of spiropyrans: Impact of isomerization dynamics at high temperatures. Chem Commun
611 2019;55:5813–6. https://doi.org/10.1039/c9cc02141h.

612 [52] Keum SR, Roh HJ, Choi YK, Lim SS, Kim SH, Koh K. Complete 1H and 13C NMR
613 spectral assignment of symmetric and asymmetric bis-spiropyran derivatives. Magn Reson
614 Chem 2005;43:873–6. https://doi.org/10.1002/mrc.1640.

615 [53] Viesser VR, Ducati LC, Tormena CF, Autschbach J. The halogen effect on the 13C
616 NMR chemical shift in substituted benzenes. Phys Chem Chem Phys 2018;20:11247–59.
617 https://doi.org/10.1039/c8cp01249k.

618 [54] Balmond EI, Tautges BK, Faulkner AL, Or VW, Hodur BM, Shaw JT, et al.
619 Comparative Evaluation of Substituent E ff ect on the Photochromic Properties of Spiropyrans
620 and Spirooxazines 2016. https://doi.org/10.1021/acs.joc.6b01193.

621 [55] Ventura C, Thornton P, Giordani S, Heise A. Synthesis and photochemical properties
622 of spiropyran graft and star polymers obtained by “click” chemistry. Polym Chem
623 2014;5:6318–24. https://doi.org/10.1039/c4py00778f.

624 [56] Trigueiro P, Pereira FAR, Guillermin D, Rigaud B, Balme S, Janot J-M, et al. When
625 anthraquinone dyes meet pillared montmorillonite: Stability or fading upon exposure to light?
626 Dye Pigment 2018;159:384–94. https://doi.org/10.1016/j.dyepig.2018.06.046.

627 [57] Hasegawa I, Takayama T, Naito S. Inorganic-organic hybrids produced from
628 tetraethoxysilane and 2-hydroxybenzyl alcohol as studied by solid-state 13C and 29Si NMR
629 spectroscopy. Mater Res Bull 1999;34:63–70. https://doi.org/10.1016/S0025-5408(98)00208-
630 6.

631 [58] Borovin E, Callone E, Ceccato R, Quaranta A, Dirè S. Adsorptive properties of sol-gel
632 derived hybrid organic/inorganic coatings. Mater Chem Phys 2014;147:954–62.
633 https://doi.org/10.1016/j.matchemphys.2014.06.042.

634 [59] Földvári M. Handbook of the thermogravimetric system of minerals and its use in
635 geological practice. vol. 56. 2011. https://doi.org/10.1556/CEuGeol.56.2013.4.6.

636 [60] da Costa Duarte R, da Silveira Santos F, de Araújo BB, Cercena R, Brondani D, Zapp

637 E, et al. Synthesis of a 5-carboxy indole-based spiropyran fluorophore: Thermal,
638 electrochemical, photophysical and bovine serum albumin interaction investigations.
639 Chemosensors 2020;8. https://doi.org/10.3390/CHEMOSENSORS8020031.

640 [61] Barrena MI, De Salazar JMG, Soria A, Matesanz L. Pre-hydrolysed ethyl silicate as an
641 alternative precursor for SiO2-coated carbon nanofibers. Appl Surf Sci 2011;258:1212–6.
642 https://doi.org/10.1016/j.apsusc.2011.09.073.

643 [62] Zheng J-Z, Zhou X-P, Xie X-L, Mai Y-W. Silica hybrid particles with nanometre
644 polymer shells and their influence on the toughening of polypropylene. Nanoscale
645 2010;2:2269–74. https://doi.org/10.1039/b9nr00344d.

646 [63] Whelan J, Abdallah D, Wojtyk J, Buncel E. Micro-environmental fine-tuning of
647 electronic and kinetic properties of photochromic dyes. J Mater Chem 2010;20:5727–35.
648 https://doi.org/10.1039/c0jm00585a.

649 [64] Xie X, Mistlberger G, Bakker E. Reversible photodynamic chloride-selective sensor
650 based on photochromic spiropyran. J Am Chem Soc 2012;134:16929–32.
651 https://doi.org/10.1021/ja307037z.

652 [65] Bergaoui L, Mrad I, Lambert J-F, Ghorbel A. A Comparative Study of the Acidity
653 toward the Aqueous Phase and Adsorptive Properties of Al 13 -Pillared Montmorillonite and
654 Al 13 -Pillared Saponite. J Phys Chem B 2002;103:2897–902.
655 https://doi.org/10.1021/jp984011e.

656 [66] Mrad I, Ghorbel A, Tichit D, Lambert JF. Optimisation of the preparation of an Al-
657 pillared clay: Thermal stability and surface acidity. Appl Clay Sci 1997;12:349–64.
658 https://doi.org/10.1016/S0169-1317(97)00018-5.

659 [67] Kortekaas L, Browne WR. The evolution of spiropyran: Fundamentals and progress of
660 an extraordinarily versatile photochrome. Chem Soc Rev 2019;48:3406–24.
661 https://doi.org/10.1039/c9cs00203k.

662 [68] Silvi S, Constable EC, Housecroft CE, Beves JE, Dunphy EL, Tomasulo M, et al.
663 Photochemical switching of luminescence and singlet oxygen generation by chemical signal
664 communication. Chem Commun 2009:1484–6. https://doi.org/10.1039/b900712a.

665 [69] Atabekyan LS, Chibisov AK. Acid effect on photochromism of spiropyrans: a study by
666 microsecond and nanosecond flash photolysis 1985;31:123–30.

667 [70] Bao B, Fan J, Wang W, Yu D. Photochromic Cotton Fabric Prepared by Spiropyran-
668 ternimated Water Polyurethane Coating. Fibers Polym 2020;21:733–42.
669 https://doi.org/10.1007/s12221-020-9749-3.

670 [71] Jozwiakowski M.J, Connors K.A. Studies on Adsorptiochromism II: Diffuse
671 Reflectance Spectroscopy of Adsorptiochromic Spiropyrans Adsorbed to Some
672 Pharmaceutically Useful Solids. J Pharm Sci 1988;77:241–6.
673 https://doi.org/10.1002/jps.2600770312.

674 [72] Yariv, S., Cross, H. (1979). Colloid Geochemistry of Clay Minerals. In: Geochemistry of
675 Colloid Systems; 287-233. https://doi.org/10.1007/978-3-642-67041-1_8.

676 [73] Kinashi K., Harada Y., Ueda Y. Thermal stability of merocyanine form in
677 spiropyran/silica composite film.Thin Solid Films 2008;516:2532-2536.
678 https://doi.org/10.1016/j.tsf.2007.04.120.
679

680 [74] Cavalcanti G. R.S., Rodrigues F., Zhuang G., Balme S., Janot J-M., Fonseca, M., Jaber
681 M. Inorganic-organic hybrid pigments based on carminic acid and clay minerals. Dyes and
682 Pigments, Elsevier, 2021, 190, pp.109306. ff10.1016/j.dyepig.2021.109306ff.